Optical Properties of $(GaAs)_n$ Clusters ($n = 2-16$)

G. L. Gutsev,*,† R. H. O'Neal, Jr.,† B. C. Saha,† M. D. Mochena,† E. Johnson,‡ and C. W. Bauschlicher, Jr.§

Department of Physics, Florida A&M University, Tallahassee, Florida 32307, Environmental Sciences Institute, Florida A & M University, Tallahassee, Florida 32307, and NASA Ames Research Center, Moffett Field, California 94035

Received: April 30, 2008; Revised Manuscript Received: August 27, 2008

The electronic and geometrical structures of the lowest triplet states of $(GaAs)_n$ clusters ($n = 2-16$) are studied using density functional theory with generalized gradient approximation (DFT-GGA). It is found that the triplet-state geometries are different from the corresponding singlet-state geometries; for $n = 2-8$, 10, and 11, the triplets and singlets have different topologies, while the $(GaAs)_9$, $(GaAs)_{12}$, $(GaAs)_{15}$, and $(GaAs)_{16}$ triplets possess a reduced symmetry, due to Jahn−Teller distortions. Except for GaAs, the singlet states are the ground states. Excitation energies and oscillator strengths are computed for excitations from the ground state to ten singlet states of all $(GaAs)_n$ clusters using time-dependent density functional theory. The adiabatic singlet−triplet gap is compared to the vertical gap, and the difference in the eigenvalues of the highest-occupied and lowest-unoccupied molecular orbitals (the HOMO−LUMO gap). While these three values show large oscillations for small n, they approach each other as the cluster size grows. Thus, the HOMO−LUMO gap computed using the DFT-GGA approach presents a rather reliable estimate of the adiabatic singlet−triplet gap.

I. Introduction

Nanosized GaAs quantum dots have many potential applications that include optoelectronic sensors,[1,2] in vivo imaging for medical diagnostics,[3] quantum computing,[4] solar cells,[5] and nonlinear optics.[6] Because injection of Mn into GaAs produces diluted magnetic semiconductors,[7] doped GaAs nanoparticles are expected to be useful in spin-based electronics[8] or spintronics.

With numerous possible applications, $(GaAs)_n$ clusters have been the subjects of a number of experimental and computational studies. On the experimental side, photoionization of neutral Ga_nAs_m ($n + m = 5-25$) have shown[9] even−odd alternation in ionization properties of these clusters. Photofragmentation of positively charged $Ga_nAs_m^+$ ($n + m \leq 31$) have shown[10] these clusters to lose one or a few atoms rather than splitting into large fragments. Photoabsorbtion spectra and static electric dipole polarizabilies were obtained for Ga_nAs_m ($n + m = 4-80$)[11] and Ga_nAs_m ($n + m = 5-30$),[12,13] respectively. Photodetachment spectra are reported[14] for small $Ga_nAs_m^-$ anions ($n + m \leq 5$).

Theoretical studies were performed using different methods for singlet states of Ga_nAs_m ($n + m \leq 16$) and $(GaAs)_n$ ($n \leq 9$) clusters. Graves and Scuseria[15] studied $(GaAs)_n$ ($n = 2-4$); Lou et al.[16] studied Ga_nAs_m ($n + m \leq 10$); Liao and Balasubramanian[17] computed the structure of $(GaAs)_2$; Andreoni[18] studied $(GaAs)_n$ ($n = 2-5$); Song et al.[19] studied $(GaAs)_n$ ($n = 2-4$); Yi[20] studied $(GaAs)_n$ ($n = 2-6$); Zhao et al.[21−23] studied $(GaAs)_4$, $(GaAs)_6$, and $(GaAs)_8$; Costales et al.[24] studied $(GaAs)_n$ ($n = 1-3$); BelBruno[25] studied Ga_nAs_m ($n + m \leq 8$); Sun et al.[26] studied $(GaAs)_8$; Karamanis et al.[27] studied $(GaAs)_n$ ($n = 2-6,8$); Zhao et al.[28] studied $(GaAs)_n$ ($n = 2-9$); Feng et al.[29] studied Ga_nAs_m ($n + m \leq 16$); Karamanis et al.[6] studied $(GaAs)_n$ ($n = 2-9$). We reported[30] the results of computations on doped $(GaAs)_mMn_n$ and $(GaAs)_mFe_n$ ($m = 2-4$, $n = 0-3$).

Electric dipole polarizabilities and/or hyperpolarizabilities of $(GaAs)_n$ have been studied by several groups. Korambath and Karna[31] computed dynamic (hyper)polarizabilities of Ga_nAs_m (n, $m = 1,3,4$); Torrens[32] computed static polarizabilities of $(GaAs)_n$ for $n = 2-8$ at assumed geometries; Lan et al.[33] considered dynamic (hyper)polarizabilities of Ga_mAs_n for $n + m \leq 10$; Karamanis et al.[27] and Zhao et al.[28] computed static polarizabilities of $(GaAs)_n$ for $n = 2-6$, 8 and $n = 2-9$, respectively; Maroulis et al.[34,35] performed a detailed study of dynamic hyperpolarizability of $(GaAs)_2$ and differential polarizabilities of $(GaAs)_n$ clusters for $n = 2-5$.

In our previous work,[36] we focused on the singlet states of $(GaAs)_n$ and the structure of their positively and negatively charged ions for $n = 2-15$. The work described in this manuscript concentrates on optical properties $(GaAs)_n$ ($n = 2-16$) and the adiabatic values of the singlet−triplet gap, which require an additional search for the lowest energy triplet states. These detailed triplet calculations confirmed that the GaAs clusters, excluding the dimer, have a singlet ground state. To aid future work on optical excitations of GaAs-based Q-dots, we report the excitation energies and oscillator strengths (f values) to the 10 lowest excited singlet states computed using the time-dependent density functional theory (TDDFT) technique.[37−39] Finally, we note that GaAs has a $^3\Sigma^-$ ground state, so the loss of GaAs could leave the product $(GaAs)_{n-1}$ cluster in the triplet state, which is studied in the present work.

II. Computational Details

Computations were performed using the Gaussian 03[40] program systems using the 6-311+G* basis set[41] (16s14p6d)/[9s8p3d] for the all-electron calculations and the cc-pVDZ-PP basis set[42] (8s7p7d)/[4s3p2d] for the 10-core electron

* To whom correspondence should be addressed. E-mail: gennady.gutsev@famu.edu.
† Department of Physics, Florida A&M University.
‡ Environmental Sciences Institute, Florida A & M University.
§ Mail Stop 203-3, NASA Ames Research Center.

10.1021/jp803888k CCC: $40.75
Published on Web 10/04/2008

TABLE 1: Comparison of the GaAs Ground-State Spectroscopic Constants Obtained Using Different Methods and Two Basis Sets with Experimental Data

GaAs, $^3\Sigma^-$						
basis	6-311+G*			6-311+G(3df)		
method	r_e (Å)	ω_e (cm^{-1})	D_0 (eV)	r_e (Å)	ω_e (cm^{-1})	D_0 (eV)
BPW91	2.59	205.9	2.03	2.58	206.9	2.08
B3PW91	2.57	213.1	1.98	2.56	214.2	2.02
B3LYP	2.59	206.3	2.01	2.58	207.2	2.06
TPSSTPSS	2.58	208.9	2.08	2.57	209.9	2.12
MP2	2.59	211.6	1.44	2.53	224.8	1.78
CCSD(T)	2.61	203.8	1.49	2.55	218.1	1.85
exptl[a]	2.53 ± 0.02	215	2.06± 0.05	2.53 ± 0.02	215	2.06 ± 0.05

[a] Reference 44.

TABLE 2: Comparison of the BPW91-, B3PW91-, B3LYP-, and TSSPTSSP-TDDFT Excitation Energies and Oscillator Strengths Obtained for the $(GaAs)_4$ Ground State Using the 6-311+G* Basis Set and Geometries Optimized at the Corresponding Level of Theory[a]

$(GaAs)_4$ $^1A_g(C_i)$										
BPW91			B3PW91			B3LYP			TSSPTSSP		
state	ΔE	f	state	ΔE	f	state	ΔE	A	state	ΔE	f
^1A_g	1.70	0	^1A_g	1.77	0	^1A_g	1.78	0	^1A_g	1.75	0
^1A_u	1.90	8	^1A_u	2.06	8	^1A_u	1.93	7	^1A_u	2.03	8
^1A_g	2.10	0	^1A_g	2.24	0	^1A_g	2.11	0	^1A_g	2.24	0
^1A_u	2.17	208	^1A_u	2.27	175	^1A_u	2.26	156	^1A_u	2.26	273
^1A_g	2.36	0	^1A_g	2.51	0	^1A_g	2.36	0	^1A_g	2.52	0
^1A_u	2.57	100	^1A_u	2.75	95	^1A_u	2.63	86	^1A_u	2.72	133
^1A_u	2.74	15	^1A_g	2.91	0	^1A_g	2.88	0	^1A_u	2.80	23
^1A_g	2.75	0	^1A_u	2.94	21	^1A_u	2.91	134	^1A_g	2.81	0
^1A_g	2.87	0	^1A_g	3.04	0	^1A_g	2.98	0	^1A_g	2.96	0
^1A_u	2.94	173	^1A_u	3.08	182	^1A_u	3.06	66	^1A_u	3.07	219
$\alpha_{cluster}$	5.06			4.98			5.13			4.99	
$\Delta\varepsilon$	1.44			2.42			2.46			1.49	
time	3.32.32			3.58.38			3.45.02			5.39.00	

[a] State is the final excited state, ΔE the excitation energy in eV, f the oscillator strength, $\alpha_{cluster}$ the static electric dipole polarizability per atom $[^1/_3(\alpha_{xx}+\alpha_{yy}+\alpha_{zz})/8]$ in Å^3, $\Delta\varepsilon = \varepsilon_{LUMO} - \varepsilon_{HOMO}$ the HOMO−LUMO gap in eV, time in hours.minutes.seconds for the TDDFT computation with *N*states = 10 on the same node (Pentium IV, 1867 MHz).

ECP10MDF[43] calculations of $(GaAs)_n$ clusters with $n > 9$. For $(GaAs)_9$, computations are performed using both variants to estimate the reliability of the ECP approach.

Since experimental spectroscopic constants are known[44] for the ground X $^3\Sigma^-$ state of GaAs, calibration calculations are performed using the pure DFT BPW91,[45,46] the hybrid HF-DFT[47,48] functionals B3PW91 and B3LYP,[49] the recently developed[50] τ-dependent gradient-corrected TPSSTPSS functional along with post-HF second order perturbation theory[51] (MP2), and coupled-cluster with singles and doubles and noniterative triples CCSD(T)[52,53] methods.

To evaluate the influence of basis set extension, we performed the same set of calculations using the 6-311+G(3df) basis set (16s14p8d1f)/[9s8p5d1f]. The results of these calibration calculations are presented in Table 1. As is seen, the results of the computations provide rather similar spectroscopic constants when the 6-311+G* basis set is used with the best fit to the experiment at the B3PW91 level. Augmenting the basis set leads to a better agreement with the experiment for the post-HF methods, while hardly affecting the results of the DFT-based methods.

To evaluate the BPW91, B3PW91, B3LYP, and TPSSTPSS functionals in the TDDFT computations, we chose the ground-state $(GaAs)_4$ cluster of C_i symmetry and used the 6-311+G* basis. As is seen from Table 2, all 4 methods provide the same order of the excited states except for swapping of the closely spaced seventh and eighth excited states (^1A_u and ^1A_g) at the hybrid HF-DFT levels of theory. The excitation energies obtained using all 4 methods are rather similar, with the largest deviation smaller than 0.2 eV. The largest difference in the static electric dipole polarizabilities is 0.15 Å^3 (about 3%). The difference in the orbital energies of the highest-occupied molecular orbital and lowest-unoccupied molecular orbital (the HOMO−LUMO gap) is similar for the BPW91 and TPSSTPSS approaches and for the two hybrid HF-DFT approaches; however, the partial inclusion of the Hartree−Fock exchange results in the gap for the hybrid HF-DFT functionals differing significantly from that for the BPW91 and TPSSTPSS functionals. Since our next goal is to dope the $(GaAs)_n$ clusters with 3d metal clusters, we chose the BPW91 functional because this functional is stable[54] in vibrational frequency calculations that allow the use of standard integration grids. We have also found[54] that the BPW91 functional is superior to the B3LYP with multiple transition metals. The BPW91/6-311+G* and BPW91/cc-pVDZ-PP levels of theory were calibrated for GaAs in our previous study.[36] It was found that the ECP results are in good agreement with the all-electron results.

As previously discussed,[6] there are many low-lying structures for each $(GaAs)_n$ cluster, and therefore finding the ground state can be very challenging. While a quasi-random generation of geometries would seem to avoid any possible bias in the starting geometries, it is not practical. We therefore maximize the possibility of finding the true ground-state structure by starting the geometry optimizations from a number of different initial

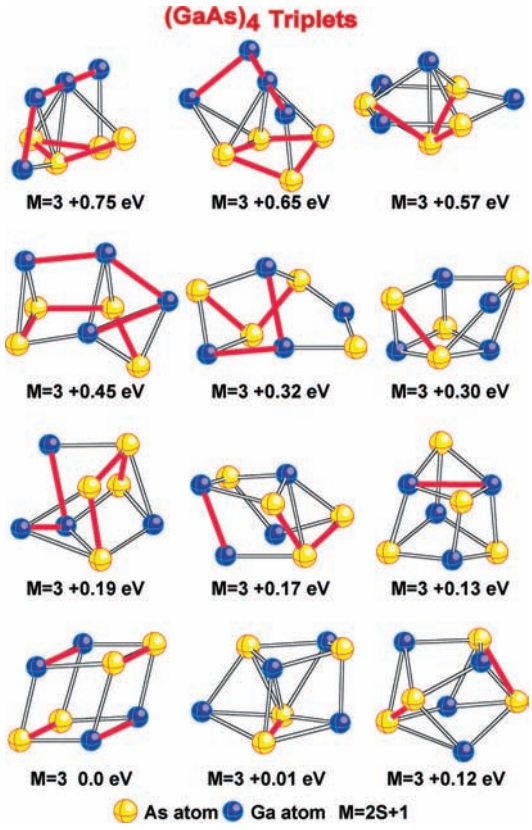

Figure 1. The lowest-energy triplet states optimized for $(GaAs)_4$. Red wide lines show the bonds between atoms of the same type.

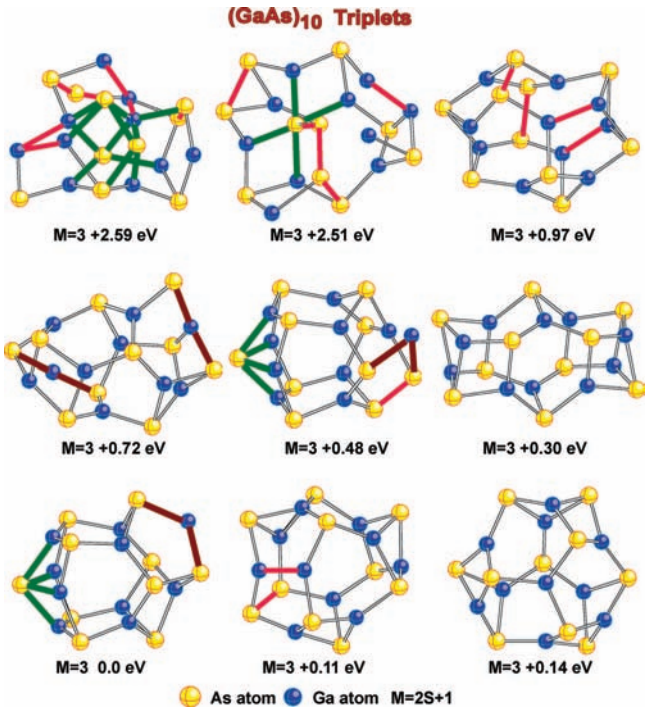

Figure 2. The lowest-energy triplet states optimized for $(GaAs)_{10}$. Red wide lines show the bonds between atoms of the same type; brown and green lines show bonds for two- and four-coordinate atoms.

geometries that span a large number of shapes but still account for the nature of the bonding. These include various $(GaAs)_n$ singlet and ion geometries obtained in our previous search, which include the topologies of isovalent $(BN)_n$ clusters that were studied by Strout[55,56] for $n = 8-12$, $(GaAs)_n$ geometries published in the works of others, adding GaAs units to smaller

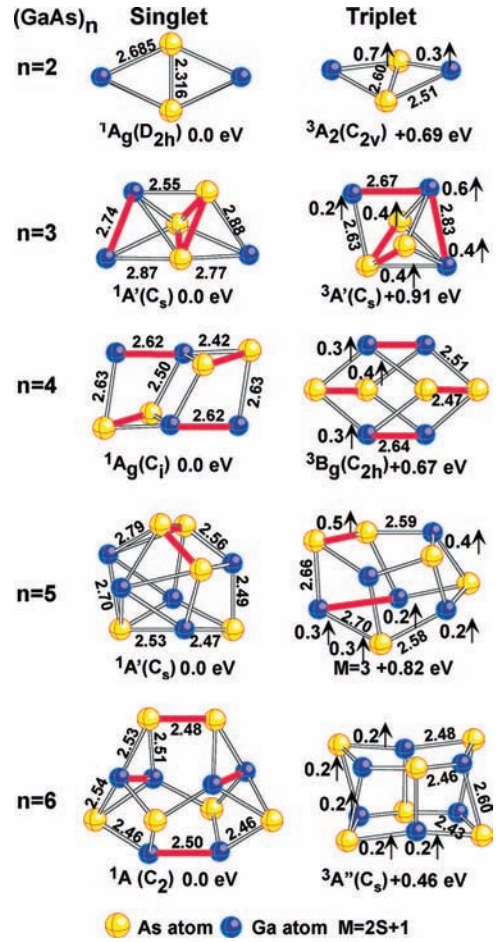

Figure 3. The ground singlet and lowest-energy triplet states of $(GaAs)_n$ for $n = 2-6$.

clusters, deleting GaAs units from larger clusters, and bulklike clusters that were formed by cutting different pieces from zinc blend lattice. One should note that, unlike carbon fullerenes[57] that are composed of hexagons and 12 pentagons, $(BN)_n$ and $(GaAs)_n$ fullerenes are composed of hexagons and rhombi if only B−N (or Ga−As) bonds are allowed. These fullerenes contain exactly 6 rhombi; the number of hexagons is $n - 4$, except for $n = 5$, where no fullerene structure exists. We also optimized structures containing Ga_2As_3 and As_2Ga_3 pentagons. Each geometry optimization was followed by an analytical second derivatives calculation of the harmonic vibrational frequencies to confirm that the optimized geometry corresponds to a minimum. In most cases, a dozen or more trial geometries were used in our search for the geometries of the lowest energy states.

The adiabatic singlet−triplet separations are computed at the DFT level and include the zero-point vibrational energies (ZPVE). For the vertical singlet−triplet separation, we use the TDDFT approach because of convergence problems for some triplet states at the high symmetry singlet geometries. We computed excess electron spin densities at the atoms in the triplet states using the Mulliken[58] population analysis. The excess electron spin densities obtained using the natural bond orbital code[59] based on natural atomic orbitals are essentially the same.

III. Results and Discussion

First, we present the geometrical configurations for the lowest triplet states of the $(GaAs)_n$ clusters for $n = 2-16$, which we compare with our previous results for the singlet states (n.b.

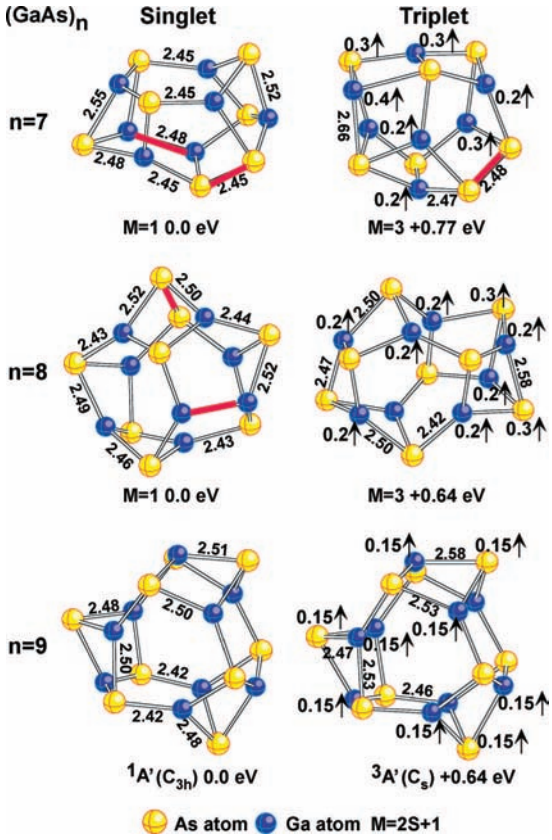

Figure 4. The ground singlet and lowest-energy triplet states of $(GaAs)_n$ for $n = 7-9$.

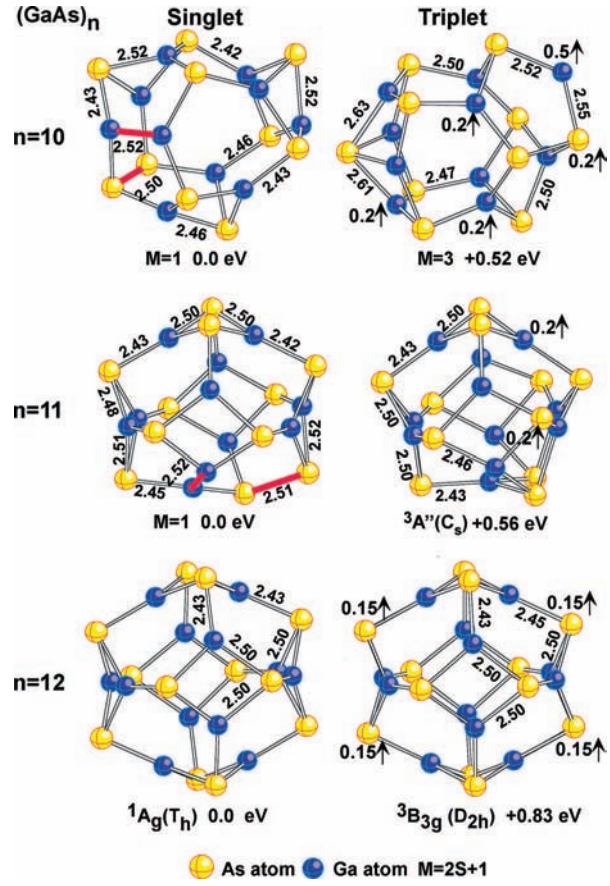

Figure 5. The ground singlet and lowest-energy triplet states of $(GaAs)_n$ for $n = 10-12$.

the singlet state for $n = 16$ was not reported previously). Next, we present the results of our TDDFT computations for the singlet−singlet excitations and adiabatic singlet−triplet excitation energies.

To gain insight in the inhomogenuity of the electronic distributions, we show in Figures 3−7 the excess electron spin densities of the atoms that are larger than 0.2 e. The sum of the excess electron spin densities is equal to the number of unpaired electrons and therefore is 2 for the triplet states (n.b. the sum of our values are not exactly two since values less than 0.2 e are not reported). Bond lengths are given in angstroms, with the bonds between atoms of the same type given as wide red lines. For clusters with no symmetry, we give the spin multiplicity following "M =". In Figures 3−7, the zero of energy is set to the singlet ground state.

Harmonic vibrational frequencies of the ground singlet states of the $(GaAs)_n$ clusters are rather similar and fall in the range from ~40 to 300 cm^{-1}. Vibrational frequencies of the lowest-energy triplet states shown in Figures 3−7 are smaller than those of the corresponding ground states. For example, the singlet vibrational frequencies of $(GaAs)_{15}$ fall between 42.4 and 297.3 cm^{-1}, while the triplet vibrational frequencies are between 31.6 and 287.7 cm^{-1}. Vibrational frequencies computed at the ECP level are somewhat smaller than those computed using the all-electron basis set. For example, the vibrational frequencies of singlet $(GaAs)_9$ computed at the ECP level are 3−7 cm^{-1} smaller than those computed at the all-electron level, which correlates with the bond lengths being 0.01 to 0.03 Å longer at the ECP level.

A. Geometrical Configurations. To demonstrate the complexity of the search for the lowest-energy state, we displayed the geometrical configurations of the triplet states optimized for $(GaAs)_4$ and $(GaAs)_{10}$ in Figures 1 and 2, respectively. The geometry optimizations were performed without imposing symmetry constraints, and all of the states were confirmed to be the local minima by the results of the corresponding vibrational frequency calculations. As is seen from Figure 1, there are 11 triplet states within 0.75 eV of the lowest energy triplet state, with rather different geometrical structures. Note that the lowest triplet state, which is composed of 6 rhombi, actually has C_{2h} symmetry and was reoptimized with C_{2h} constraints in Figure 3.

For the $(GaAs)_{10}$ cluster, we considered both cage and bulklike structures, where four-coordinate atoms are presented. These bulklike structures were obtained from optimizations of clusters taken from zinc blend bulk structures. As is seen, the states corresponding to both fullerenes (6 rhombi and 6 hexagons) possess higher total energy than the state whose geometry is formed by adding a dissociated GaAs dimer to the ground $(GaAs)_9$ structure. While we performed geometry optimizations starting from numerous geometries for both the singlet and triplet states, we should note that there is some possibility that we have not found the lowest states of both spins.

Figure 3 displays the lowest energy triplet states of $(GaAs)_n$ for $n = 2-6$ optimized in this work along with the singlet ground-state structures determined previously. The singlet and triplets have different geometric structures; in some cases the difference is relatively small, while in others there are significant changes. Consider the case of $(GaAs)_6$, where the singlet has a structure with three Ga−Ga bonds and one As−As bond, while the triplet has only Ga−As bonds. The excess spin densities are distributed rather inhomogeneuosly. For example, in $(GaAs)_3$, one Ga has an excess spin of 0.6 e, while another has only 0.2 e, and one pair of As atoms has 0.4 e, while one As

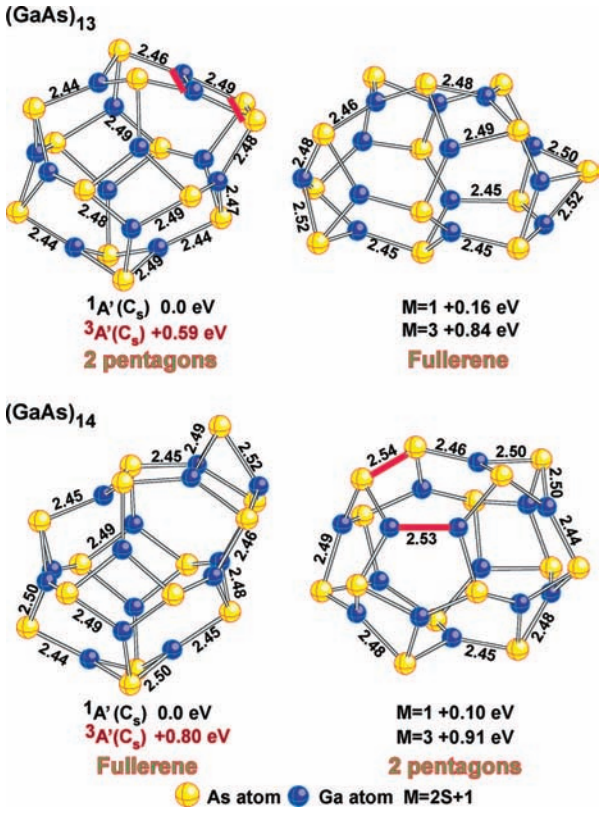

Figure 6. Two lowest-energy singlet and triplet states of $(GaAs)_{13}$ and $(GaAs)_{14}$.

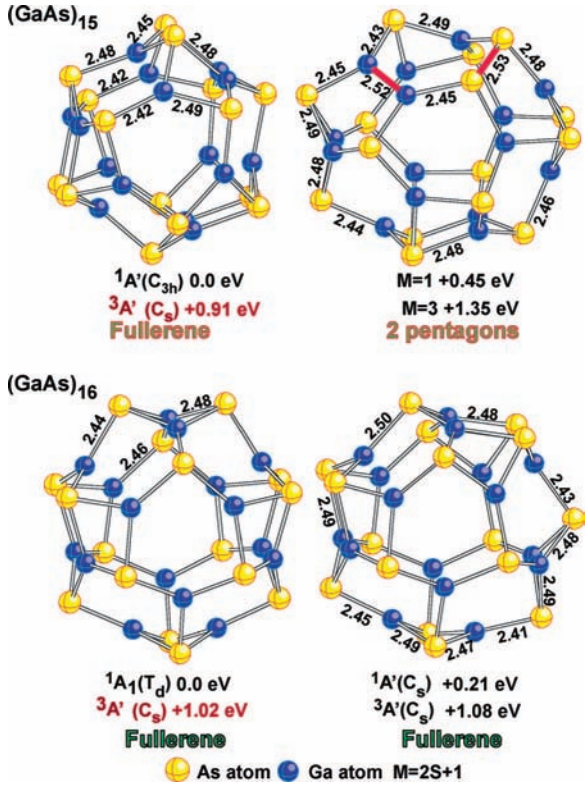

Figure 7. Two lowest-energy singlet and triplet states of $(GaAs)_{15}$ and $(GaAs)_{16}$.

has no essential excess spin. The triplet state of $(GaAs)_6$ has the geometrical structure composed of 6 rhombi and 2 hexagons and represents the smallest BN-type fullerene.

The lowest-energy triplet of $(GaAs)_7$ has one pair of Ga_3As_2 pentagons, in contrast with the singlet ground state that has two pairs of Ga_2As_3 and Ga_3As_2 pentagons, see Figure 4. The lowest triplet state of $(GaAs)_8$ has a fullerene topology comprised of 3 pairs of edge-sharing rhombi separated by 4 hexagons while the singlet ground state has two pairs of Ga_2As_3 and Ga_3As_2 pentagons. However, it should be noted that the singlet fullerene structure is only 0.02 eV higher in energy. While the singlet fullerene has S_4 symmetry, the symmetry is lower for the triplet state, and our optimizations were performed without imposing symmetry constraints. Strout[55] found a similar fullerene topology for the $(BN)_8$ singlet ground state. The ground-state geometrical structure of $(GaAs)_9$ is similar to that found by Strout[56] for $(BN)_9$ and possesses a fullerene topology. The triplet state of $(GaAs)_9$ has a similar geometrical configuration that is slightly distorted to C_s symmetry due to the Jahn−Teller effect.

The lowest-energy triplet state of $(GaAs)_{10}$ has one four-coordinate As atom and one two-coordinate Ga atom that carry a rather large excess spin density (see Figure 5). The singlet state with the same topology is higher than the singlet ground-state by 0.12 eV, while the lowest-energy singlet state with a fullerene topology is above the ground-state by 0.26 eV. These energies are to be compared to the corresponding triplet energies presented in Figure 2.

The lowest-energy triplet state of $(GaAs)_{11}$ has a fullerene geometry shown in Figure 5. This is different from the singlet ground-state structure that includes two pairs of Ga_2As_3 and Ga_3As_2 pentagons. However, there is a singlet fullerene structure that is only 0.02 eV above the ground state. Such a fullerene structure, where six four-member rings are arranged as two edge-sharing pairs and two isolated rhombi, is also found[55] for the ground-state of $(BN)_{11}$. The $(GaAs)_{12}$ ground-state geometry has a fullerene topology similar[55,60,61] to that of $(BN)_{12}$. It has T_h symmetry where 6 rhombi are all separated by 8 hexagons. The lowest-energy triplet state of $(GaAs)_{12}$ has a fullerene geometry as well, but it has lower symmetry due to a Jahn−Teller distortion.

Both ground singlet and lowest-energy triplet states of $(GaAs)_{13}$ have geometrical configurations that contain one Ga_2As_3 and one Ga_3As_2 pentagon (see Figure 6). The triplet (singlet) state with a fullerene geometrical configuration is 0.25 eV (0.16 eV) above the two-pentagon structure. Thus, $(GaAs)_{13}$ is somewhat different from the smaller clusters, where the triplet states favor the fullerene structure relative to the singlet states. $(GaAs)_{14}$ is different again, with both its triplet and singlet states favoring a fullerene structure of C_s symmetry with 2 edge-sharing rhombi and 4 separated rhombi. A similar ground-state topology was found[62] for $(BN)_{14}$ as well. The singlet and triplet states with two pairs of Ga_2As_3 and Ga_3As_2 pentagons are 0.10 and 0.11 eV, respectively, above the fullerene.

The singlet ground-state of $(GaAs)_{15}$ has the topology of a fullerene with 6 separated rhombi and possess C_{3h} symmetry (see Figure 7). The lowest-energy triplet state has a similar structure, but its symmetry is reduced to C_s due to a Jahn−Teller distortion. The singlet and triplet states of $(GaAs)_{15}$ with the geometrical configuration containing two pairs of Ga_2As_3 and Ga_3As_2 pentagons are 0.45 and 0.44 eV, respectively, above their fullerene counterparts.

The ground-state of $(GaAs)_{16}$ has the fullerene topology presenting a truncated octahedron, similar to that found[63,64] for $(BN)_{16}$. The lowest energy triplet state geometry has the same topology, but its symmetry is reduced to C_s. The singlet and triplet states possessing a fullerene topology of C_s symmetry with 6 separated rhombi but placed differently than in the T_d fullerene are higher in energy by 0.21 and 0.06 eV, respectively (see Figure 7). The singlet and triplet states possessing a

TABLE 3: Transition Energies (in eV) and *f* Values ($\times 10^4$) for the Ten Lowest Singlet States from the Ground-State $(GaAs)_n$ Clusters Obtained from All-Electron TDDFT Computations

state	ΔE	f	state	ΔE	f	state	ΔE	f	state	ΔE	f
	$(GaAs)_2$			$(GaAs)_3$			$(GaAs)_4$			$(GaAs)_5$	
^1A_u	1.33	0	$^1A'$	**2.34**	77	^1A_g	1.69	0	$^1A'$	**1.89**	22
$^1B_{2g}$	1.53	0	$^1A''$	2.53	11	^1A_u	**1.89**	8	$^1A'$	2.01	25
$^1B_{1g}$	2.60	0	$^1A'$	2.57	10	^1A_g	2.09	0	$^1A''$	2.12	2
$^1B_{3u}$	**2.67**	276	$^1A''$	2.62	9	^1A_u	2.16	127	$^1A'$	2.13	46
$^1B_{1g}$	3.23	0	$^1A''$	2.75	1	^1A_g	2.36	0	$^1A'$	2.28	26
$^1B_{3g}$	3.37	0	$^1A'$	3.10	42	^1A_u	2.57	66	$^1A''$	2.32	25
^1A_u	3.52	0	$^1A''$	3.25	0	^1A_u	2.74	12	$^1A'$	2.37	14
$^1B_{1u}$	3.57	107	$^1A''$	3.43	6	^1A_g	2.74	0	$^1A''$	2.37	12
$^1B_{2g}$	3.63	0	$^1A'$	3.48	119	^1A_g	2.86	0	$^1A'$	2.45	57
$^1B_{2u}$	3.81	176	$^1A''$	3.55	0	^1A_u	2.93	117	$^1A''$	2.47	25
	$(GaAs)_6$			$(GaAs)_7$			$(GaAs)_8$			$(GaAs)_9$	
^1B	**1.23**	9	^1A	**1.49**	6	^1A	**1.12**	13	$^1A'$	0.94	0
^1A	1.39	0	^1A	1.60	25	^1A	1.34	19	$^1E''(2)$	1.00	0
^1A	1.49	21	^1A	1.75	13	^1A	1.40	17	$^1E'(2)$	**1.29**	32×2
^1A	1.54	3	^1A	1.95	3	^1A	1.64	2	$^1E''(2)$	1.53	0
^1B	1.64	26	^1A	2.02	0	^1A	1.73	8	$^1A''$	1.75	48
^1B	1.77	100	^1A	2.10	6	^1A	1.77	2	$^1A'$	1.78	0
^1A	1.88	2	^1A	2.12	1	^1A	1.81	35	$^1E'(2)$	1.81	75×2
^1B	2.03	15	^1A	2.24	70	^1A	1.90	8	$^1E''(2)$	2.14	0
^1B	2.10	3	^1A	2.30	45	^1A	2.00	13	$^1A''$	2.16	5
^1A	2.26	4	^1A	2.31	18	^1A	2.01	21	$^1E'(2)$	2.31	88×2

TABLE 4: Transition Energies (in eV) and *f* Values ($\times 10^4$) for the Ten Lowest Singlet States from the Ground-State $(GaAs)_n$ Clusters Obtained from ECP TDDFT Computations

state	ΔE	f	state	ΔE	f	state	ΔE	f	state	ΔE	f
	$(GaAs)_9$			$(GaAs)_{10}$			$(GaAs)_{11}$			$(GaAs)_{12}$	
$^1A'$	1.03	0	^1A	**1.14**	12	^1A	**1.08**	8	$T_g(3)$	1.00	0
$^1E''(2)$	1.12	0	^1A	1.29	21	^1A	1.17	11	$E_u(2)$	1.42	0
$^1E'(2)$	**1.39**	29×2	^1A	1.40	8	^1A	1.38	8	$T_u(3)$	**1.47**	7×3
$^1E''(2)$	1.65	0	^1A	1.46	5	^1A	1.44	17	$T_g(3)$	1.59	0
$^1A'$	1.85	0	^1A	1.53	4	^1A	1.52	13	$T_u(3)$	2.13	226×3
$^1A''$	1.88	41	^1A	1.60	10	^1A	1.63	15	$T_g(3)$	2.30	0
$^1E'(2)$	1.91	74×2	^1A	1.73	13	^1A	1.65	18	$E_g(2)$	2.38	0
$^1E''(2)$	2.25	0	^1A	1.80	18	^1A	1.74	1	$T_u(3)$	2.44	21×3
$^1A''$	2.31	9	^1A	1.89	50	^1A	1.85	10	$T_g(3)$	2.67	0
$^1E'(2)$	2.43	64×2	^1A	1.94	30	^1A	1.95	8	$T_g(3)$	2.75	0.015(3)
	$(GaAs)_{13}$			$(GaAs)_{14}$			$(GaAs)_{15}$			$(GaAs)_{16}$	
$^1A'$	**1.19**	140	$^1A''$	**0.99**	1	$^1E''(2)$	1.04	0	$T_1(3)$	1.12	0
$^1A''$	1.32	11	$^1A'$	1.00	24	$^1A'$	1.25	0	$T_1(3)$	1.38	0
$^1A''$	1.42	1	$^1A''$	1.17	1	$^1A''$	**1.41**	20	$^1A_2$	1.65	0
$^1A'$	1.51	8	$^1A'$	1.30	38	$^1E'(2)$	1.54	6×2	$T_2(3)$	**1.88**	24×3
$^1A''$	1.55	18	$^1A'$	1.48	7	$^1E''(2)$	1.56	0	$^1E(2)$	1.88	0
$^1A''$	1.68	0	$^1A''$	1.50	11	$^1A''$	1.63	0	$T_1(3)$	1.92	0
$^1A'$	1.73	16	$^1A''$	1.53	6	$^1E''(2)$	1.69	0	$T_2(3)$	2.14	17×3
$^1A''$	1.82	1	$^1A''$	1.56	6	$^1A''$	1.81	5	$^1A_1$	2.24	0
$^1A'$	1.83	0	$^1A'$	1.57	3	$^1E'(2)$	1.87	9×2	$T_2(3)$	2.31	246×3
$^1A'$	1.88	59	$^1A''$	1.60	6	$^1E'(2)$	2.14	51×2	$T_1(3)$	2.50	0

geometry that contains one Ga_2As_3 pentagon and one Ga_3As_2 pentagon (similar to $(GaAs)_{13}$ shown in Figure 6) are higher by 0.78 and 0.38 eV, respectively.

B. Optical Properties and Singlet−Triplet Separations. The results of the triplet-state optimizations of this work combined with our previous results on the singlet states[36] do confirm that the small $(GaAs)_n$ clusters have the singlet ground states, except for the GaAs dimer whose ground state is a triplet. Therefore, we compute only the singlet−singlet optical transitions using the TDDFT approach. We should note that the TDDFT results have previously been reported for the smaller GaAs clusters: Vasiliev et al.[65,66] computed optical excitations of Ga_nAs_m clusters for $n + m \leq 10$ using a local spin density approximation (LSDA), while Zhao et al.[28] used the Perdew−Burke−Ernzerhof (PBE) exchange correlation potential for $(GaAs)_n$ ($n = 2 - 9$).

Our TDDFT calculations for the first 10 singlet−singlet transitions were performed at the geometries of the ground singlet states. The all-electron BPW91/6-311+G* level is used for $n = 2-9$, while the ECP BPW91/cc-pVDZ-PP level is used for $n = 9-16$; the results are presented in Tables 3 and 4, respectively. Comparison of the values obtained for $(GaAs)_9$ using both approaches reveals that the ECP transition energies are nearly uniformly shifted by 0.1 eV to larger values. For the high-symmetry species, many transitions have zero *f* values, as expected, due to the electric dipole selection rules. For the smaller clusters, our values for the first transition energy are similar to those obtained by Zhao et al.[28] The lowest excitation energy oscillates for the smaller clusters, settling down to 1.07 $\pm$ 0.13 eV by $n = 8$. The lowest-energy transitions with nonzero *f* values are given in bold in the tables. They start off at 2.67 eV for $(GaAs)_2$ and decease rapidly with increasing cluster size, such that by $n = 6$ the value is about 1.2 $\pm$ 0.2 eV, with exceptions for $(GaAs)_7$ (1.49 eV), which is just outside this range, and the high-symmetry $(GaAs)_{16}$ (1.88 eV), which is

TABLE 5: Properties of $(GaAs)_n$ Clusters Computed at the BPW91/6-311+G* Level for $n = 2-9$ and ECP10MDF/cc-pVDZ-PP Level for $n = 9-16$

		all electron								effective core							
	n	2	3	4	5	6	7	8	**9**	9	10	11	12	13	14	15	16
S−S transition[a], eV		2.67	2.34	1.89	1.89	1.23	1.49	1.12	**1.29**	1.39	1.14	1.08	1.47	1.19	1.00	1.41	1.88
	HOMO−LUMO	1.26	2.10	1.44	1.76	1.18	1.32	1.06	**0.98**	0.88	1.08	1.03	0.99	1.03	0.97	1.02	1.11
Δ(S−T) eV	vertical	1.09	1.79	1.23	1.62	1.13	1.20	1.00	**0.91**	0.81	0.99	0.97	0.96	0.95	0.93	0.99	1.09
	adiabatic	0.69	0.91	0.67	0.87	0.46	0.77	0.64	**0.64**	0.66	0.52	0.56	0.83	0.59	0.80	0.91	1.02

[a] S−S transition is the energy of the first singlet−singlet transition with nonzero *f* value.

significantly larger. The strength of the transitions is quite variable: in general, the lowest allowed transitions are weak, but there are exceptions, for example, for $(GaAs)_2$ and $(GaAs)_{13}$, where the first allowed transition is the strongest one. As noted by Zhao et al.,[28] for the clusters $(GaAs)_9$ and smaller, the transitions vary significantly from cluster to cluster, and that is also true for the larger clusters considered in this work.

The singlet−triplet separations are computed using three approaches: the adiabatic values are obtained as the difference in total energies of the singlet ground-state and the lowest-energy triplet states, which are given in the figures, the vertical values obtained using the TDDFT method, and as the difference between the eigenvalues of the highest occupied and lowest unoccupied molecular orbitals for the singlet ground state. These three sets of the results are given in Table 5. Given the difference in the singlet and triplet geometries, the difference between the vertical and adiabatic values is not unexpected. However, the use of the TDDFT approach, used to avoid convergence problems, for the vertical value could also be contributing to some of the difference. The vertical value appears to be converging to a value of about 1.1 eV (n.b. the ECP values should be increased by about 0.1 eV). The HOMO−LUMO gap is in reasonable agreement with the vertical value and supports its use in qualitative studies,[67] where $(GaAs)_n$ clusters up to $n = 100$ were studied using a tight-binding DFT approximation and assumed geometries.

As the cluster size increases, it might be expected that the singlet−triplet separation and the energy of the first dipole-allowed singlet−singlet transition would converge to the bulk value of 1.424 eV. While our vertical singlet−triplet separation and first dipole-allowed singlet−singlet transition are relatively stable for clusters bigger than $(GaAs)_6$, the larger singlet−singlet value for $(GaAs)_{16}$ suggest that still larger clusters are required to approach the bulk limit for these properties.

IV. Summary and Conclusions

The results of our computations performed using density functional theory with generalized gradient approximation (DFT-GGA) for the triplet and singlet states of the $(GaAs)_n$ clusters for $n = 2-16$ allow the following conclusions:

(i) All of the $(GaAs)_n$ clusters for $n > 1$ have a singlet ground state.

(ii) All atoms in the ground-state geometries of $(GaAs)_n$ for $n > 5$ are three coordinate, and there is a competition between the states possessing fullerene geometries, comprised from hexagons and rhombi, and the states whose geometrical structures contain Ga_2As_3 and Ga_3As_2 pentagons. The notable exception is presented by the lowest energy triplet state of $(GaAs)_{10}$ where one atom is four coordinate and another one is two coordinate.

(iii) In general, the triplet states favor the fullerene structure more than the singlet states.

(iv) The vertical singlet−triplet separation obtained using the TDDFT method rapidly converges to about 1 eV with increasing cluster size. Since the singlet and triplet states have different geometries in general, the adiabatic singlet−triplet separation is smaller, although the difference appears to be decreasing with the cluster size.

(v) The energy of the lowest dipole allowed singlet−singlet transition initially decrease with increasing cluster size, reaching a value of 1.2 ± 0.2 eV by $(GaAs)_6$, with exceptions for $(GaAs)_7$ (1.49 eV) and $(GaAs)_{16}$ (1.88 eV).

Our prediction of singlet ground states for these clusters is probably best tested using an electron spin resonance experiment, which should detect any unpaired electrons. The experimental confirmation of the singlet geometrical structure could be obtained using the ionization energy reported in our previous paper and the electronic excitation energies and *f* values reported in this work. We hope that the results obtained in this and previous work will encourage experimentalists to study these fundamentally interesting GaAs clusters.

Acknowledgment. This research was partly supported by the ML Program of U.S. Air Force AFRL Contract No. FA8650-05-D-1912, by the National Science Foundation, CREST program (Grant 0630370), and by funding from the National Oceanic and Atmospheric Administration (NOAA) of the United States Department of Commerce to the Environmental Sciences Institute at Florida A & M University (NOAA Award No. NA05OAR4811018). We are very thankful to Drs. Kirk Peterson and George Maroulis for instructive discussions.

References and Notes

(1) Chen, W.; Zhang, J. Z.; Joly, A. G. *J. Nanosci. Nanotech.* **2004**, *4*, 919.
(2) Costa-Fernández, J. M.; Pereiro, R.; Sanz-Medel, A. *Trends Anal. Chem.* **2006**, *25*, 207.
(3) Michalet, X.; Pinaud, F. F.; Bentolila, L. A.; Tsay, J. M.; Doose, S.; Li, J. J.; Sundaresan, G.; Wu, A. M.; Gambhir, S. S.; Weiss, S. *Science* **2005**, *538*, 2007.
(4) Calarco, T.; Datta, A.; Fedichev, P.; Pazy, E.; Zoller, P. *Phys. Rev. B* **2003**, *68*, 012310.
(5) Schaller, R. D.; Klimov, V. I. *Phys. Rev. Lett.* **2006**, *96*, 097402.
(6) Karamanis, P.; Bégué, D.; Pouchan, C. *J. Chem. Phys.* **2007**, *127*, 094706.
(7) Ohno, H.; Shen, A.; Matsukura, F.; Oiwa, A.; Endo, A.; Katsumoto, S.; Iye, Y. *Appl. Phys. Lett.* **1996**, *69*, 363.
(8) Wolf, S. A.; Awschalom, D. D.; Buhrman, R. A.; Daughton, J. M.; von Molnár, S.; Roukes, M. L.; Chtchelkanova, A. Y.; Treger, D. M. *Science* **2001**, *294*, 1488.
(9) O'Brien, S. C.; Liu, Y.; Zhang, Q.; Heath, J. R.; Tittel, F. K.; Curl, R. F.; Smalley, R. E. *J. Chem. Phys.* **1986**, *84*, 4074.
(10) Zhang, Q.-L; Liu, Y.; Curl, R. F.; Tittel, F. K.; Smalley, R. E. *J. Chem. Phys.* **1987**, *88*, 1670.
(11) Schäfer, R.; Becker, J. A. *Phys. Rev. B* **1996**, *54*, 10296.
(12) Schlecht, S.; Schiifer, R.; Woenckhaus, J.; Becker, J. A. *Chem. Phys. Lett.* **1995**, *246*, 315.
(13) Schäfer, R.; Schlecht, S.; Woenckhaus, J.; Becker, J. A. *Phys.Rev. Lett.* **1996**, *76*, 471.
(14) Taylor, T. R.; Gómez, H.; Asmis, K. R.; Neumark, D. M. *J. Chem. Phys.* **2001**, *115*, 4620.

(15) Graves, R. M.; Scuseria, G. E. *J. Chem. Phys.* **1991**, *95*, 6602.
(16) Lou, L.; Wang, L.; Chibante, L. P. F.; Laaksonen, R. T.; Nordlander, P.; Smalley, R. E. *J. Chem. Phys.* **1991**, *94*, 8015.
(17) Liao, D. W.; Balasubramanian, K. *J. Chem. Phys.* **1992**, *96*, 8938.
(18) Andreoni, W. *Phys. Rev. B* **1992**, *45*, 4203.
(19) Song, K. M.; Ray, A. K.; Khowash, P. K. *J. Phys. B: At. Mol. Opt. Phys.* **1994**, *27*, 1637.
(20) Yi, J.-Y. *Chem. Phys. Lett.* **2000**, *325*, 269.
(21) Zhao, W.; Cao, P.-L.; Li, B.-X.; Song, B. *Phys. Rev. B.* **2000**, *62*, 17138.
(22) Zhao, W.; Cao, P.-L. *Phys. Lett. A* **2001**, *288*, 53.
(23) Zhao, W.; Cao, P.-L.; Duan, W. *Phys. Lett. A* **2006**, *349*, 224.
(24) Costales, A.; Kandalam, A. K.; Franco, R.; Pandey, R. *J. Phys. Chem. B* **2002**, *106*, 1940.
(25) BelBruno, J. J. *Heteroatom Chem.* **2003**, *14*, 189.
(26) Sun, Y.; Chen, X.; Sun, L.; Guo, X.; Lu, W. *Chem. Phys. Lett.* **2003**, *381*, 397.
(27) Karamanis, P.; Begué, D.; Pouchan, C. *Comp. Lett.* **2006**, *2*, 255.
(28) Zhao, J.; Xie, R.-H.; Zhou, X.; Chen, X.; Lu, W. *Phys. Rev. B* **2006**, *74*, 035319.
(29) Feng, Y. P.; Boo, T. B.; Kwong, H. H.; Ong, C. K.; Kumar, V.; Kawazoe, Y. *Phys. Rev. B* **2007**, *76*, 045336.
(30) Gutsev, G. L.; Mochena, M. D.; Bauschlicher, C. W., Jr *Chem. Phys. Lett.* **2007**, *439*, 95.
(31) Korambath, P. P.; Karna, S. P. *J. Phys. Chem. A* **2000**, *104*, 4801.
(32) Torrens, F. *Physica E* **2002**, *13*, 67.
(33) Lan, Y.-Z.; Cheng, W.-D.; Wu, D.-S.; Shen, J.; Huang, S.-P.; Zhang, H.; Gong, Y.-J.; Li, F.-F. *J. Chem. Phys.* **2006**, *124*, 094302.
(34) Maroulis, G.; Karamanis, P.; Pouchan, C. *J. Chem. Phys.* **2007**, *126*, 154316.
(35) Karamanis, P.; Pouchan, C.; Maroulis, G. *Phys. Rev. A* **2008**, *77*, 013201.
(36) Gutsev, G. L.; Johnson, E; Mochena, M. D.; Bauschlicher, C. W., Jr *J. Chem. Phys.* **2008**, *128*, 144707.
(37) Casida, M. E.; Jamorski, C.; Casida, K. C.; Salahub, D. R. *J. Chem. Phys.* **1998**, *108*, 4439.
(38) Burke, K.; Werschnik, J.; Gross, E. K. U. *J. Chem. Phys.* **2005**, *123*, 062206.
(39) Wang, F.; Ziegler, T.; van Lenthe, E.; van Gisbergen, S.; Baerends, E. J. *J. Chem. Phys.* **2005**, *123*, 204103.
(40) Frisch, M. J.; Trucks, G. W.; Schlegel, H. B.; Scuseria, G. E.; Robb, M. A.; Cheeseman, J. R.; Montgomery, J. A., Jr.; Vreven, T.; Kudin, K. N.; Burant, J. C.; Millam, J. M.; Iyengar, S. S.; Tomasi, J.; Barone, V.; Mennucci, B.; Cossi, M.; Scalmani, G.; Rega, N.; Petersson, G. A.; Nakatsuji, H.; Hada, M.; Ehara, M.; Toyota, K.; Fukuda, R.; Hasegawa, J.; Ishida, M.; Nakajima, T.; Honda, Y.; Kitao, O.; Nakai, H.; Klene, M.; Li, X.; Knox, J. E.; Hratchian, H. P.; Cross, J. B.; Bakken, V.; Adamo, C.; Jaramillo, J.; Gomperts, R.; Stratmann, R. E.; Yazyev, O.; Austin, A. J.; Cammi, R.; Pomelli, C.; Ochterski, J. W.; Ayala, P. Y.; Morokuma, K.; Voth, G. A.; Salvador, P.; Dannenberg, J. J.; Zakrzewski, V. G.; Dapprich, S.; Daniels, A. D.; Strain, M. C.; Farkas, O.; Malick, D. K.; Rabuck, A. D.; Raghavachari, K.; Foresman, J. B.; Ortiz, J. V.; Cui, Q.; Baboul, A. G.; Clifford, S.; Cioslowski, J.; Stefanov, B. B.; Liu, G.; Liashenko, A.; Piskorz, P.; Komaromi, I.; Martin, R. L.; Fox, D. J.; Keith, T.; Al-Laham, M. A.; Peng, C. Y.; Nanayakkara, A.; Challacombe, M.; Gill, P. M. W.; Johnson, B.; Chen, W.; Wong, M. W.; Gonzalez, C.; Pople, J. A. *Gaussian 03*, revision D.01; Gaussian, Inc.: Wallingford, CT, 2004.
(41) Curtiss, L. A.; McGrath, M. P.; Blaudeau, J.-P.; Davis, N. E.; Binning, R. C., Jr.; Radom, L. *J. Chem. Phys.* **1995**, *103*, 6104.
(42) Peterson, K. A. *J. Chem. Phys.* **2003**, *119*, 11099.
(43) Metz, B.; Stoll, H.; Dolg, M. *J. Chem. Phys.* **2000**, *113*, 2563.
(44) Lemire, G. W.; Bishea, G. A.; Heidecke, S. A.; Morse, M. D. *J. Chem. Phys.* **1990**, *92*, 121.
(45) Becke, A. D. *Phys. Rev. A* **1988**, *38*, 3098.
(46) Perdew, J. P.; Wang, Y. *Phys. Rev. B* **1992**, *45*, 13244.
(47) Becke, A. D. *J. Chem. Phys.* **1993**, *98*, 5648.
(48) Lee, C.; Yang, W.; Parr, R. G. *Phys. Rev. B* **1988**, *37*, 785.
(49) Stephens, P. J.; Devlin, F. J.; Chabalowski, C. F.; Frisch, M. J. *J. Phys. Chem.* **1994**, *98*, 11623.
(50) Tao, J. M.; Perdew, J. P.; Staroverov, V. N.; Scuseria, G. E. *Phys. Rev. Lett.* **2003**, *91*, 146401.
(51) Head-Gordon, M.; Pople, J. A.; Frisch, M. J. *Chem. Phys. Lett.* **1988**, *153*, 503.
(52) Urban, M.; Noga, J.; Cole, S. J.; Bartlett, R. J. *J. Chem. Phys.* **1985**, *83*, 4041.
(53) Pople, J. A.; Head-Gordon, M.; Raghavachari, K. *J. Chem. Phys.* **1987**, *87*, 5968.
(54) Gutsev, G. L.; Mochena, M. D.; Bauschlicher, C. W., Jr *J. Phys. Chem. A* **2003**, *107*, 7013.
(55) Strout, D. L. *J. Phys. Chem. A* **2000**, *104*, 3364.
(56) Strout, D. L. *J. Phys. Chem. A* **2001**, *105*, 261.
(57) Dresselhaus, M. S.; Dresselhaus, G.; Eklund, P. C. *J. Mater. Res.* **1993**, *8*, 2045.
(58) Mulliken, R. S. *J. Chem. Phys.* **1955**, *23*, 1833, 1841, 2338,2343.
(59) Reed, A. E.; Curtiss, L. A.; Weinhold, F. *Chem. Rev.* **1988**, *88*, 899.
(60) Sun, M.-L.; Slanina, Z.; Lee, S.-L. *Chem. Phys. Lett.* **1995**, *233*, 279.
(61) Seifert, G.; Fowler, R. W.; Mitchell, D.; Porezag, D.; Frauenheim, Th. *Chem. Phys. Lett.* **1997**, *268*, 352.
(62) Strout, D. L. *Chem. Phys. Lett.* **2004**, *383*, 95.
(63) Alexandre, S. S.; Chacham, H.; Nunes, R. W. *Phys. Rev. B* **2001**, *63*, 045402.
(64) Moon, W. H.; Son, M. S.; Hwang, H. J. *Appl. Surf. Sci.* **2007**, *253*, 7078.
(65) Vasiliev, I.; Ögüt, S.; Chelikowsky, J. R. *Phys. Rev. B* **2002**, *65*, 115416.
(66) Vasiliev, I.; Ögüt, S.; Chelikowsky, J. R. *Phys. Rev. B* **1999**, *60*, R8477.
(67) Ghosh, C.; Pal, S.; Goswami, B.; Sarkar, P. *Chem. Phys. Lett.* **2005**, *407*, 498.

JP803888K